# Multimode electron transport through quantum waveguides with spin-orbit interaction modulation: Applications of the scattering matrix formalism

Lebo Zhang,[1,2,*] P. Brusheim,[1,†] and H. Q. Xu[1,‡]
[1]*Division of Solid State Physics, Lund University, Box 118, S-22100 Lund, Sweden*
[2]*Department of Physics, Dalian University of Technology, Dalian 116024, China*
(Received 6 December 2004; revised manuscript received 17 May 2005; published 21 July 2005)

We present a formulation of the scattering matrix method for spin-dependent electron transport in a quantum waveguide with spin-orbit interaction (SOI). All the required Hamiltonian matrices needed in the implementation of the formulation are represented in a basis of the transverse spatial eigenstates and the spin eigenstates of the leads. Thus the method has great flexibility and can be easily applied to systems with complex geometrical structure, potential distribution, and SOI strength profile. Also, the method is numerically stable and can be used to treat spin-dependent multisubband scattering processes accurately. We have applied the method to the spin-dependent electron transport in quasi-one-dimensional (Q1D) conductors, with a region of the Rashba SOI of uniform strength and with a region containing a Rashba SOI superlattice, made from a semiconductor heterostructure. The total conductance, spin-dependent conductances, and spin polarization of the system are calculated for a fully spin-polarized electron beam injected from a lead into the SOI region. For the Q1D conductor with a single region of the Rashba SOI, it is found that when the Fermi energy is set at a value, for which the total conductance is at a plateau, the spin-dependent conductances show regular oscillations with increasing SOI strength. This is approximately true even when the total conductance is at a high plateau and thus multiple subbands in the waveguide are open for conduction. However, when the Fermi energy is set at a value close to the onset of a subband (with the subband index $n \geqslant 2$), the spin-polarized conductances plotted against the SOI strength and the SOI region length show sharp resonance features or complex fluctuations. These irregular conductance characteristics arise from SOI-induced strong coupling between subbands. For the Q1D conductor modulated by an array of strong Rashba SOI stripes, the total conductance shows regular superlattice behavior, while the spin-dependent conductances show complex behavior with regions of slow oscillations and regions of rapid oscillations. As in the Q1D conductor with a single SOI region, the slow oscillations are found in the energy regions where the total conductance is at plateaus. However, the rapid oscillations appear at energies close to the onsets of subbands with the subband index $n \geqslant 2$. These oscillations originate from strong spin scattering by localized states formed in the SOI-modulated superlattice region.

DOI: 10.1103/PhysRevB.72.045347 PACS number(s): 73.23.Ad, 71.70.Ej, 72.10.−d, 72.25.−b

## I. INTRODUCTION

The ballistic electron spin-transport phenomena have attracted recent attention[1–12] due to their potential applications in the design of spintronic devices. The main challenge in the field of spintronics is to achieve the injection, modulation, and detection of electron spin in nanometer scale structures. In 1990, Datta and Das[13] proposed a spin transistor which is an analog of the standard electro-optic light modulator. In their model, ferromagnetic contacts were used as spin-polarized source and detector, and the electron spin was manipulated via the Rashba spin-orbit interaction (SOI). The SOI is a relativistic effect due to an effective magnetic field experienced by electrons when moving through an electric field. This electric field can, e.g., be due to structural (Rashba) or crystal (Dresselhaus) inversion asymmetry in the device. These asymmetries will lift the electron spin-degeneracy for nonvanishing momentum creating spin-split energy bands even when no external magnetic field is present. In a two-dimensional electron gas (2DEG) system the dominating term is the Rashba SOI, arising from the inversion asymmetry of the quantum well. This interaction can also be tuned by an applied gate voltage perpendicular to the well. This control of the interaction, which was first employed by Datta and Das in their proposed spin transistor, opens the possibility to modulate the electron spin state.

The pioneering development of spintronics requires a proper theoretical model to discover and to understand transport phenomena with SOI. Recent extensive theoretical work has thus been devoted to the study of these phenomena.[2–9] In Refs. 2 and 3, discrete lattice models and the recursive Green's function technique were used to study the properties of electron transport in quasi-one-dimensional (Q1D) quantum wires with SOI. The numerical results showed a perfect spin modulation of conductance when intersubband interactions were neglected. With intersubband interactions included, the modulation deviated from the usual sinusoidal characteristics expected from a single-subband model. Spin transport in Q1D structures was also studied with continuous wave models and the transfer/scattering-matrix formalism.[4–7] However, in most of these studies, the calculations were made by taking only the two lowest subbands into account. This has the benefit of producing analytical two-band dispersion relations of the Hamiltonian, but has a drawback of neglecting the influence of higher subbands on the conductance. Such influences could further affect the spin modulation of the conductance as well as give rise to interesting new

 

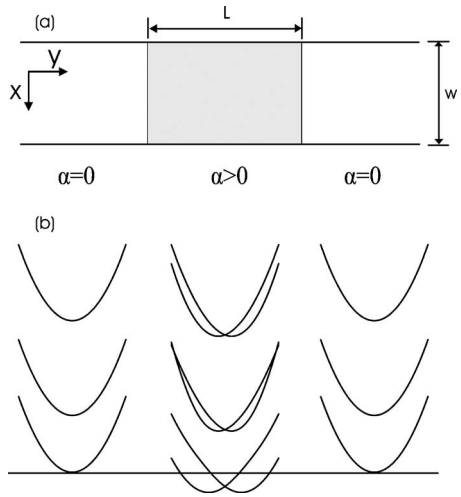


FIG. 1. (a) Schematic illustration of a Q1D conductor with a SOI region (shaded). (b) Typical dispersion relations of infinite leads and for a uniform SOI region of infinite length. The spin degeneracy in the leads is lifted in the SOI region for $k \neq 0$. The energy bands in the SOI region are also lowered due to the effective potential well created by the SOI.

features, such as resonances, due to band-mixing and interference.

In this paper, we present a continuous-wave, multimode, scattering-matrix formalism to model spin-dependent electron transport in a quantum waveguide with SOI in the linear-response regime and at zero temperature. In our model, we consider the quantum waveguide created in a 2DEG by a transverse confining potential. We will only take the Rashba SOI into account in the formulation. Incorporation of the Dresselhaus SOI in our model is straightforward. By SOI we will thus hereafter refer to the Rashba spin-orbit interaction. In the formalism, all the Hamiltonian matrices are represented in a common basis of the transverse spatial eigenstates and the spin eigenstates of the leads. Thus our method can be used to treat spin-dependent multisubband scattering processes accurately. The method can also be implemented in the study of spin devices with a complex structure and SOI profile with little numerical effort.

The paper is organized as follows. In Sec. II, the scattering-matrix formalism for multimode spin-dependent transport in a 2DEG waveguide structure is presented. In Sec. III, we apply this formalism to the problems of spin-dependent transport through a Q1D conductor with a region of SOI modulation and through a Q1D conductor with a region of a SOI superlattice. Finally, the paper is summarized and concluded in Sec. IV.

## II. MODEL AND FORMALISM

The system under consideration [see Fig. 1(a) for a schematic illustration] is a 2DEG defined in a semiconductor heterostructure with growth direction along the $z$ axis. The 2DEG, lying in the $x$-$y$ plane, is restricted to a Q1D quantum conductor of width $w$ by a transverse confining potential $V_c(x)$. The electrons transport ballistically in the conductor along the longitudinal $y$ direction. The single-particle Hamiltonian of the system under the effective mass approximation with SOI is given by

$$H = \frac{\mathbf{p}^2}{2m^*} + V_c(x) + V_E(\mathbf{r}) + \frac{1}{2\hbar}[\alpha(\mathbf{r})(\boldsymbol{\sigma} \times \mathbf{p}) + (\boldsymbol{\sigma} \times \mathbf{p})\alpha(\mathbf{r})]_z, \tag{1}$$

where $\mathbf{p}$ is the momentum operator, $m^*$ the effective mass, $V_c(x)$ the confining potential, $V_E(\mathbf{r})$ a general spin-independent potential inside the conductor, $\alpha(\mathbf{r})$ the SOI strength which is proportional to the heterostructure-interfacial electric field, taken to be in the $z$-direction, and $\boldsymbol{\sigma}$ the Pauli matrix vector. The Hamiltonian has been symmetrized in order to be Hermitian when the interaction strength is spatially dependent.[14,15] For a constant interaction strength, the form commonly found in the literature is obtained. In the leads, we let $\alpha=0$ and $V_E=0$, and assume that the eigensolutions to the transverse part of the Schrödinger equation are known and are represented by eigenvectors $|n\rangle$ with eigenvalues $\epsilon_n$. The electron eigenwave functions in the leads can in general be written in the form of $e^{iky}|n\sigma\rangle$, where $|n\sigma\rangle = |n\rangle|\sigma\rangle$ with $\sigma = \pm 1$, and $|1\rangle = (1,0)^T$ and $|-1\rangle = (0,1)^T$ representing, respectively, the spin-up and spin-down states in the $\sigma_z$ spin-representation. In the conductor region of $\alpha \neq 0$ and $V_E \neq 0$, we will solve the system by discretizing the conductor along the transport $y$ direction into $N$ transverse stripes. Assuming that each stripe is sufficiently narrow in width, so that the potential $V_E$ and the SOI strength $\alpha$ can approximately be considered to be $y$ independent, the electron eigensolutions in this stripe can be solved by expanding the wave function as

$$|\Psi\rangle = e^{iky} \sum_{n,\sigma} d_n^\sigma |n\sigma\rangle. \tag{2}$$

Here we require the states to be normalized so that $\Sigma_{n\sigma}|d_{n\beta}^\sigma|^2 = 1$. Inserting the above equation into the Schrödinger equation defined by the Hamiltonian, Eq. (1), leads to

$$\sum_{n,\sigma} \left[ \left( E - \epsilon_n - \frac{\hbar^2 k^2}{2m^*} \right) \delta_{mn}^{\sigma'\sigma} - V_{mn}\delta^{\sigma'\sigma} + \left( \sigma \eta_{mn} + \frac{\sigma}{2}\chi_{mn} - k\alpha_{mn} \right) \delta^{\sigma',-\sigma} \right] d_n^\sigma = 0, \tag{3}$$

with

$$V_{mn} = \langle m|V_E(\mathbf{r})|n\rangle,$$

$$\eta_{mn} = \langle m|\alpha(\mathbf{r})\frac{\partial}{\partial x}|n\rangle,$$

$$\chi_{mn} = \langle m|\frac{\partial \alpha(\mathbf{r})}{\partial x}|n\rangle,$$

$$\alpha_{mn} = \langle m|\alpha(\mathbf{r})|n\rangle,$$

where $V_E(\mathbf{r})$ and $\alpha(\mathbf{r})$ may, respectively, be approximated as $V_E(x,y')$ and $\alpha(x,y')$ with $y'$ being some coordinate along

the $y$ direction within the stripe. From Eq. (3), we see that the SOI introduces mixing between the spin states as well as mixing between the subbands. This implies that spin and subband indices originally used in the lead regions are not good quantum numbers in the SOI region and the electron eigenstates should, in general, be written in the form of the expansion of Eq. (2). Equation (3) can be solved for eigenenergies $E_n$ for a given $k$ value to obtain the dispersion relations, $E_n(k)$, of the system [see Fig. 1(b) for examples].

However, in an electron transport problem, Eq. (3) has to be solved for $k$ as an eigenvalue problem for a given electron energy $E$. This can be implemented in an expanded basis[16,17] as follows. By introducing auxiliary coefficients, $f^{\sigma}_{n\beta}=k_{\beta}d^{\sigma}_{n\beta}$, we can rewrite Eq. (3) as

$$\begin{pmatrix} \mathbf{0} & \mathbf{1} \\ \mathbf{S} & \mathbf{T} \end{pmatrix}\begin{pmatrix} \mathbf{D} \\ \mathbf{F} \end{pmatrix} = k_{\beta}\begin{pmatrix} \mathbf{D} \\ \mathbf{F} \end{pmatrix}, \tag{4}$$

with

$$(\mathbf{S})^{\sigma'\sigma}_{mn} = \frac{1}{\mu}\Bigg[ (E-\epsilon_n)\delta^{\sigma'\sigma}_{mn} - V_{mn}\delta^{\sigma'\sigma} + \left(\sigma\eta_{mn}+\frac{\sigma}{2}\chi_{mn}\right)\delta^{\sigma',-\sigma}\Bigg],$$

$$(\mathbf{T})^{\sigma'\sigma}_{mn} = -\frac{\alpha_{mn}}{\mu}\delta^{\sigma',-\sigma},$$

$$(\mathbf{D})^{\sigma}_{n\beta} = d^{\sigma}_{n\beta}, \tag{5}$$

and $\mu=\hbar^2/2m^*$. For a given energy $E$, Eq. (4) gives a set of eigenwave numbers, $k_{\beta}$, and a set of corresponding eigenvectors, $d^{\sigma}_{n\beta}$, within each stripe.

It is important to notice that because of the SOI induced translational shift in $k$-space of the dispersion relations [see Fig. 1(b)], propagation direction of an eigenstate in the SOI region cannot be identified by the sign of its eigenwave number. Instead, the mean velocity needs to be used to determine the propagation direction of the eigenstate. Here it should be emphasized that proper determination of the propagation directions of all the eigenstates of the system is a critical step in implementation of the scattering-matrix formalism for a multimode waveguide. Using the velocity operator derived directly from the Hamiltonian,

$$\hat{v}_y = \frac{i}{\hbar}[H,y] = \frac{p_y}{m^*} + \frac{\alpha(\mathbf{r})}{\hbar}\sigma_x, \tag{6}$$

we can calculate the expectation value of $\hat{v}_y$ for the eigenstate corresponding to the eigenwave number $k_{\beta}$ as

$$\langle\hat{v}_y\rangle_{\beta} = \sum_{m\sigma' n\sigma} (d^{\sigma'}_{m\beta})^{*}\langle m\sigma'|\frac{\hbar k_{\beta}}{m^*} + \frac{\alpha(\mathbf{r})}{\hbar}\sigma_x|n\sigma\rangle d^{\sigma}_{n\beta}. \tag{7}$$

When $k_{\beta}$ is real, $\mathrm{Re}\langle\hat{v}_y\rangle_{\beta}$ is known as the quantum mean velocity of the state with wave number $k_{\beta}$.

In line with Ref. 17, we divide the set of eigenwave numbers into two subsets. The first subset consists of wave numbers, $\{k_{I\beta}\}$, which are complex but have a positive imaginary part, or which are real and whose corresponding eigenstates have a positive mean velocity. The second subset consists of wave numbers, $\{k_{II\beta}\}$, which are complex and have a negative imaginary part, or which are real and whose corresponding eigenstates have a negative mean velocity. The eigenstates in the first subset are those which are evanescent or propagating in the forward direction and the eigenstates in the second subset are those which are exploding or backward propagating. Note that the two subsets have an equal number of elements.

In order to solve for the full wave function of an electron at energy $E$ for the entire system, we now write the wave function in stripe $j$ as

$$|\Psi^j\rangle = \sum_{\beta n\sigma}[d^{(j)\sigma}_{In\beta}a^{(j)}_{I\beta}e^{ik^j_{I\beta}(y-y^j_0)} + d^{(j)\sigma}_{IIn\beta}a^{(j)}_{II\beta}e^{ik^j_{II\beta}(y-y^j_0)}]|n\sigma\rangle, \tag{8}$$

where $y^j_0$ is some reference coordinate for stripe $j$. Since the choice of $y^j_0$ is arbitrary, i.e., the calculation for electron transport should not depend on the choice of $y^j_0$, we can choose a set of $y^j_0$, such that $y^L_0=y^1_0$, $y^R_0=y^{N+1}_0$, and $y^{j+1}_0-y^j_0=l^j$, where $l^j$ is the width of stripe $j$. The continuity requirements on the electron probability density and flux density at the interface between stripes $j$ and $j+1$, i.e., $\Psi^j|_{y=y^{j+1}_0} = \Psi^{j+1}|_{y=y^{j+1}_0}$ and $(\hat{v}^j_y\Psi^j)|_{y=y^{j+1}_0} = (\hat{v}^{j+1}_y\Psi^{j+1})|_{y=y^{j+1}_0}$, lead to a set of linear equations relating the wave function expansion coefficients in stripe $j$ with those in stripe $j+1$,

$$\begin{pmatrix} \mathbf{A}^j_I \\ \mathbf{A}^j_{II} \end{pmatrix} = \mathbf{M}(j,j+1)\begin{pmatrix} \mathbf{A}^{j+1}_I \\ \mathbf{A}^{j+1}_{II} \end{pmatrix}, \tag{9}$$

where $\mathbf{A}^j_I$ and $\mathbf{A}^j_{II}$ are the vectors containing $\{a^{(j)}_{I\beta}\}$ and $\{a^{(j)}_{II\beta}\}$, respectively, and

$$\mathbf{M}(j,j+1) = \begin{pmatrix} \mathbf{\Gamma}^j_I & \mathbf{0} \\ \mathbf{0} & \mathbf{\Gamma}^j_{II} \end{pmatrix}^{-1}\begin{pmatrix} \mathbf{P}^j_I & \mathbf{P}^j_{II} \\ \mathbf{Q}^j_I & \mathbf{Q}^j_{II} \end{pmatrix}^{-1}\begin{pmatrix} \mathbf{P}^{j+1}_I & \mathbf{P}^{j+1}_{II} \\ \mathbf{Q}^{j+1}_I & \mathbf{Q}^{j+1}_{II} \end{pmatrix}, \tag{10}$$

with

$$(\mathbf{\Gamma}^j_I)_{\beta\beta} = e^{ik^j_{I\beta}l^j}, \quad (\mathbf{\Gamma}^j_{II})_{\beta\beta} = e^{ik^j_{II\beta}l^j},$$

$$(\mathbf{P}^j_I)^{\sigma}_{n\beta} = d^{(j)\sigma}_{In\beta}, \quad (\mathbf{P}^j_{II})^{\sigma}_{n\beta} = d^{(j)\sigma}_{IIn\beta},$$

$$(\mathbf{Q}^j_I)^{\sigma}_{n\beta} = \sum_m\left[\frac{\hbar k^j_{I\beta}}{m^*}d^{(j)\sigma}_{Im\beta}\delta_{nm} + \frac{\alpha_{nm}}{\hbar}d^{(j)-\sigma}_{Im\beta}\right],$$

$$(\mathbf{Q}^j_{II})^{\sigma}_{n\beta} = \sum_m\left[\frac{\hbar k^j_{II\beta}}{m^*}d^{(j)\sigma}_{IIm\beta}\delta_{nm} + \frac{\alpha_{nm}}{\hbar}d^{(j)-\sigma}_{IIm\beta}\right]. \tag{11}$$

The full transfer matrix, $\mathbf{M}(L,R)$, relating the coefficients of the left and right leads is found from matrix multiplication of the individual matrices connecting adjacent stripes. The transfer matrix method is prone to numerical instabilities for large systems due to the presence of the exploding terms $\{(\Gamma_{II})_{\beta\beta}\}$ in the formalism.[17,18] However, by defining a scattering matrix, $\mathbf{S}(L,R)$, relating the outgoing waves from the conductor to the incoming waves we can remove the numerical instabilities caused by the exploding terms from the cal-

culations. The system of linear equations then reads

$$\begin{pmatrix} \mathbf{A}_I^R \\ \mathbf{A}_{II}^L \end{pmatrix} = \mathbf{S}(L,R) \begin{pmatrix} \mathbf{A}_I^L \\ \mathbf{A}_{II}^R \end{pmatrix}. \tag{12}$$

The elements of the scattering matrix **S** are given in terms of elements of the transfer matrix **M**, and are readily obtainable from Eqs. (10) and (11). For a detailed derivation and explicit expressions of the scattering matrix, we refer to Refs. 17 and 18. The coefficients $\mathbf{A}_I^j$ and $\mathbf{A}_{II}^j$ at a stripe $j$ inside the conductor can easily be extracted within the scattering matrix formalism using a procedure presented in Ref. 19. This gives a means of calculating the wave function inside the conductor according to Eq. (8).

A unique solution of the Schrödinger equation of the quantum system can only be obtained after we impose a boundary condition on the electron wave function. Here we are interested in the transport properties of the system. We therefore need to consider the situation that an electron of energy $E$ is incident in subband $m$, with spin $\sigma'$, from the left lead into the conductor. In the left lead we will then have both forward and backward propagating waves, whereas in the right lead only forward propagating waves will be present. The wave function in the left and right leads can then be written as

$$|\Psi^L\rangle = e^{ik_m^{\sigma'}(y-y_0^L)}|m\sigma'\rangle + \sum_{n\sigma} a_{IIn}^{(L)\sigma} e^{ik_{IIn}^{\sigma}(y-y_0^L)}|n\sigma\rangle,$$

$$|\Psi^R\rangle = \sum_{n\sigma} a_{In}^{(R)\sigma} e^{ik_{In}^{\sigma}(y-y_0^R)}|n\sigma\rangle. \tag{13}$$

Thus the boundary condition imposed on the electron wave function is $\mathbf{A}_I^L = \mathbf{I}_m^{\sigma'}$ and $\mathbf{A}_{II}^R = \mathbf{0}$, where $(\mathbf{I}_m^{\sigma'})_n^{\sigma}$ is a unit vector with elements given by $(\mathbf{I}_m^{\sigma'})_n^{\sigma} = \langle n\sigma | m\sigma' \rangle$. Here we note that in writing the wave function in the left lead, we have explicitly written the wave vector of the incident electron as $k_m^{\sigma'}$, in order to clarify the boundary condition satisfied by the wave function. We have also added a superscript $\sigma$ to the wave vectors, $k_{In}^{\sigma}$ and $k_{IIn}^{\sigma}$, to specify the spin orientation of the transmitted and reflected waves. Inserting the boundary condition into Eq. (12) gives us the expansion coefficients of the transmitted and reflected waves,

$$\mathbf{A}_I^R = \mathbf{S}_{11}(L,R)\mathbf{I}_m^{\sigma'},$$

$$\mathbf{A}_{II}^L = \mathbf{S}_{21}(L,R)\mathbf{I}_m^{\sigma'}. \tag{14}$$

The electrical current carried by the electron state is given by

$$J(E,k_m^{\sigma'}) = -e\,\mathrm{Re}\langle \hat{v}_y \rangle, \tag{15}$$

where $e>0$ is the electron charge unit. Note that in the above equation, the mean velocity needs to be calculated with the corresponding wave function of the electron with energy $E$ and spin $\sigma'$ incident in subband $m$ from the left lead. However, the calculation does not depend on the value of $y$, as required by the current continuity condition. This allows us to simplify the evaluation of the electric current carried by the electron wave using the expression of the wave function in the right lead, where $\alpha(\mathbf{r})=0$ and $V_E(\mathbf{r})=0$. The result is

$$J(E,k_m^{\sigma'}) = -\frac{e\hbar}{m^*}\sum_{n\sigma}^{R} k_n^{\sigma}|a_{In}^{\sigma}|^2, \tag{16}$$

where $R$ denotes that the sum is taken over all states for which $k_n^{\sigma} = \sqrt{2m^*(E-\epsilon_n)}/\hbar$ is real. Here the class index, $I$, has been dropped from the wave vector $k_{In}^{\sigma}$, and superscript $(R)$ has been dropped from the expansion coefficient $a_{In}^{(R)}$. The linear-response conductance of the system at zero temperature now reads

$$G = -\frac{e}{h}\sum_{m\sigma'}^{R} \frac{J(E_F,k_m^{\sigma'})}{\hbar k_m^{\sigma'}/m^*} = \frac{e^2}{h}\sum_{m\sigma'}^{R}\sum_{n\sigma}^{R} \frac{k_n^{\sigma}|a_{In}^{\sigma}|^2}{k_m^{\sigma'}} = \sum_{m\sigma' n\sigma}^{R} G_{nm}^{\sigma\sigma'}, \tag{17}$$

where $k_n^{\sigma}|a_{In}^{\sigma}|^2/k_m^{\sigma'} \equiv T_{nm}^{\sigma\sigma'}$ is the transmission probability. Similarly we can define the reflection probability as

$$R = \sum_{m\sigma' n\sigma}^{R} R_{nm}^{\sigma\sigma'} = \sum_{m\sigma' n\sigma}^{R} \frac{k_n^{\sigma}|a_{IIn}^{\sigma}|^2}{k_m^{\sigma'}}. \tag{18}$$

Here again the superscript $(L)$ has been dropped from the expansion coefficient $a_{IIn}^{(L)}$. By not performing the sums over the spin indices $\{\sigma,\sigma'\}$ we can extract the spin-dependent conductances, $G^{\sigma\sigma'}$, and reflection probabilities, $R^{\sigma\sigma'}$, for electrons injected with spin $\sigma'$ and scattered into states with spin $\sigma$. From the spin-dependent conductances we can define the spin polarization in the $z$ direction as

$$P_z = \frac{G^{\uparrow\uparrow} + G^{\uparrow\downarrow} - G^{\downarrow\uparrow} - G^{\downarrow\downarrow}}{G^{\uparrow\uparrow} + G^{\uparrow\downarrow} + G^{\downarrow\uparrow} + G^{\downarrow\downarrow}}. \tag{19}$$

Limiting the calculation to electrons injected in spin up state only, Eq. (19) can be simplified to

$$P_z = \frac{G^{\uparrow\uparrow} - G^{\downarrow\uparrow}}{G^{\uparrow\uparrow} + G^{\downarrow\uparrow}}. \tag{20}$$

The method presented above is formulated in a basis of infinite order and is exact provided that the conductor region is divided into an infinite (or a sufficiently large) number of stripes. However, solving Eq. (4) numerically requires truncating the basis set $\{|n\sigma\rangle\}$. In the actual calculations, we will set the basis set as large as it is necessary to obtain a desired convergence in the calculated transport quantities.

## III. NUMERICAL RESULTS AND DISCUSSION

### A. Single SOI region

We now demonstrate the implementation of the formalism presented in the previous section by first applying it to a waveguide structure with a region of the SOI of uniform strength, made from an InGaAs/InAlAs heterostructure. We assume that the waveguide has a width $w$ and is defined by a hard-wall confinement potential, i.e., $V_c(x)=0$ for $x \in [0,w]$ and $\infty$ otherwise. The conductor region with the SOI is de-

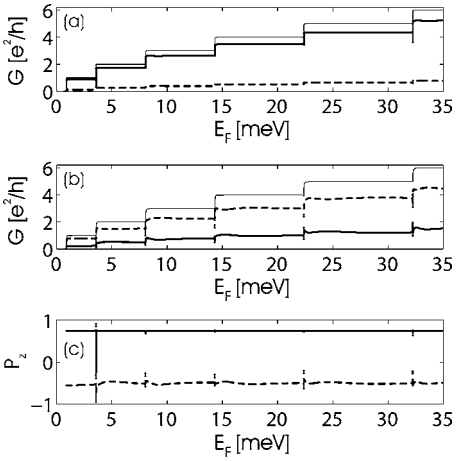


FIG. 2. Total conductance $G$ (thin solid line), spin-up conductance $G^{\uparrow\uparrow}$ (thick solid line), and spin-down conductance $G^{\downarrow\uparrow}$ (dashed line) as a function of the Fermi energy $E_F$ at (a) $\alpha=3\times10^{-12}$ eV m and (b) $\alpha=9\times10^{-12}$ eV m for electrons injected in spin-up states into the SOI region with the size of $L=220$ nm and $w=100$ nm. (c) Spin polarization $P_z$ of the system as a function of the Fermi energy $E_F$. The solid line is the result for $\alpha=3\times10^{-12}$ eV m and the dashed line is the result for $\alpha=9\times10^{-12}$ eV m.

fined inside the waveguide and has a length $L$ and the same width $w$ as the waveguide [see Fig. 1(a)]. In the calculations, we take $L=220$ nm, unless otherwise stated, and $w=100$ nm. We also assume a nonvanishing, constant, but tunable strength, $\alpha(\mathbf{r})=\alpha>0$, in the SOI region. We further assume that the electrons have an effective mass of $m^*=0.042m_e$, where $m_e$ is the free electron mass. We have calculated the total conductance, the spin-dependent conductances, spin polarization, and spin-flipped reflection for the device as a function of the Fermi energy $E_F$, the SOI strength $\alpha$, and the length $L$ of the SOI region. The results are displayed in Figs. 2–7. Here we should note that only the results of the calculations for electrons injected with spin-up polarization states from the left lead into the SOI region are presented and discussed in this work. The results of the calculations for electrons injected with the opposite spin-polarization states are identical, if the spin labels, ↑ and ↓, are interchanged.

In Figs. 2, 3(a), and 3(b), the calculated total conductance, $G$, spin-dependent conductances, $G^{\uparrow\uparrow}$ and $G^{\downarrow\uparrow}$, and spin polarization, $P_z$, of the transmitted electrons at different values of $\alpha$ are plotted against the Fermi energy $E_F$. Figure 3(c) shows the results of the calculations for the spin-flipped reflection probability, $R^{\downarrow\uparrow}$. In general, the SOI entangles the spin-up and spin-down states of an electron and will cause the electron spin to precess when the electron propagates through the SOI region. For $\alpha=3\times10^{-12}$ eV m the SOI is rather weak and the electron spin can only be slightly rotated after it passes through the SOI region. This is seen in Fig. 2(a) as a reduction in the spin-up conductance, $G^{\uparrow\uparrow}$, as well as a corresponding increase in the spin-down conductance, $G^{\downarrow\uparrow}$. However, the spin polarization, $P_z$, approximately remains at a constant and is independent of the Fermi energy [the solid line in Fig. 2(c)]. Furthermore, the total conductance, $G$, shows roughly the same quantized conductance characteristics as observed in a uniform Q1D conductor without including the SOI region. At $\alpha=9\times10^{-12}$ eV m, the similar behaviors of the conductances are found [Fig. 2(b)]. However, sharp conductance dips appear at Fermi energies close to the onset of subbands with the subband index $n\geqslant2$. These Fano-resonance type dips appear as a result of subband interaction; they can be attributed to interference between the waves which propagate via Q1D subbands through the SOI region and the waves which pass through the SOI region via bound states derived from higher subbands due to the presence of an SOI-induced effective potential well [see Fig. 1(b)].[20,21] In addition, the spin polarization, $P_z$, becomes overall negative at $\alpha=9\times10^{-12}$ eV m [the dashed line in Fig. 2(c)], which indicates that at this in-

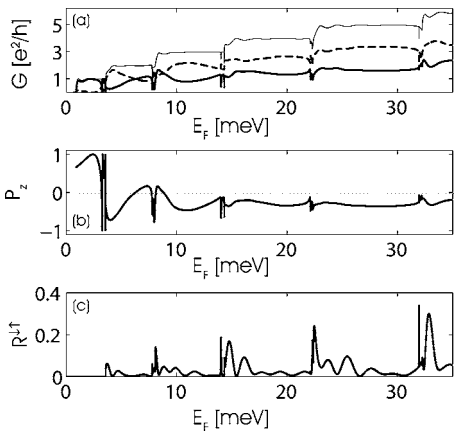


FIG. 3. (a) Total conductance $G$ (thin solid line), spin-up conductance $G^{\uparrow\uparrow}$ (thick solid line), and spin-down conductance $G^{\downarrow\uparrow}$ (dashed line) as a function of the Fermi energy $E_F$ for electrons injected in the spin-up states into the SOI region with the size of $L=220$ nm and $w=100$ nm and the SOI strength of $\alpha=33\times10^{-12}$ eV m. (b) The corresponding spin polarization $P_z$. (c) Spin-flipped reflection probability, $R^{\downarrow\uparrow}$, of the system.

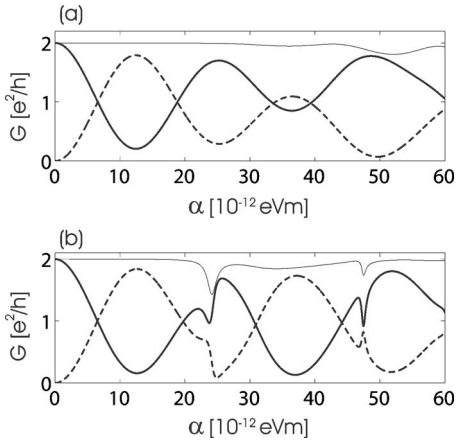


FIG. 4. Total conductance $G$ (thin solid line), spin-up conductance $G^{\uparrow\uparrow}$ (thick solid line), and spin-down conductance $G^{\downarrow\uparrow}$ (dashed line) as a function of the SOI strength $\alpha$ for electrons injected in the spin-up states into the SOI region with the size of $L=220$ nm and $w=100$ nm at (a) the Fermi energy $E_F=6.5$ meV and (b) the Fermi energy $E_F=7.9$ meV.

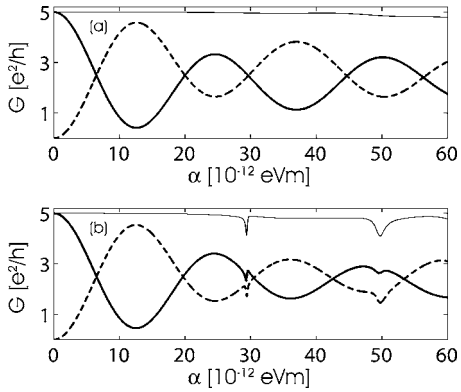


FIG. 5. Total conductance $G$ (thin solid line), spin-up conductance $G^{\uparrow\uparrow}$ (thick solid line), and spin-down conductance $G^{\downarrow\uparrow}$ (dashed line) as a function of the SOI strength $\alpha$ for electrons injected in the spin-up states into the SOI region with the size of $L=220$ nm and $w=100$ nm at (a) the Fermi energy $E_F=28.5$ meV and (b) the Fermi energy $E_F=32$ meV.

creased SOI strength the electron spin has been rotated more than 90° after it goes through the SOI region.

For a further increased SOI strength, the conductance and spin-polarization spectra tend to show complex structures, due to the presence of strong coupling between subbands. In Fig. 3(a) the results of the calculations for the interaction strength $\alpha=33\times10^{-12}$ eV m are plotted. For this strong interaction, the total conductance maintains its good quantized conductance shape, but the two spin-dependent conductances show large variations or oscillations. These oscillations appear to be particularly strong around subband edges (except the first one), where strong and complicated subband couplings are expected to appear.[22] The calculated spin polarization as shown in Fig. 3(b) also exhibits large variations and strong oscillations, differing from the weak SOI strength cases as shown in Fig. 2(c). We would like to emphasize again that the appearance of the spin-dependent conductance oscillations and spin-polarization oscillations is a clear deviation from the prediction of a single-subband model and they can only be found when a multisubband coupling model is employed. Figure 3(c) shows that the spin-flipped reflection is significantly strong at energies close to subband edges (except for the lowest one). It was noted in Ref. 5 that spin-flipped reflection should not occur. This was argued because the reflected electron will rotate its spin back when traveling in the opposite direction. However, this is only true for the particular conditions studied in Ref. 5, i.e., when only one subband is open for conduction. When multiple subbands are open for transmission the electron can travel back in different subbands. Since the speed at which the spin rotates is different for different subbands, the electron will not necessarily end up in its original spin state, resulting in a nonvanishing spin-flipped reflection amplitude.

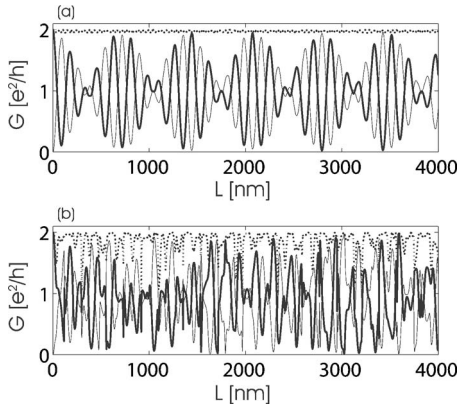


FIG. 6. Total conductance $G$ (dotted line), spin-up conductance $G^{\uparrow\uparrow}$ (thick solid line), and spin-down conductance $G^{\downarrow\uparrow}$ (thin solid line) as a function of the length $L$ of the SOI region with the width $w=100$ nm and the SOI strength $\alpha=33\times10^{-12}$ eV m: (a) the results for the Fermi energy at $E_F=6.5$ meV and (b) the results for the Fermi energy $E_F=7.9$ meV.

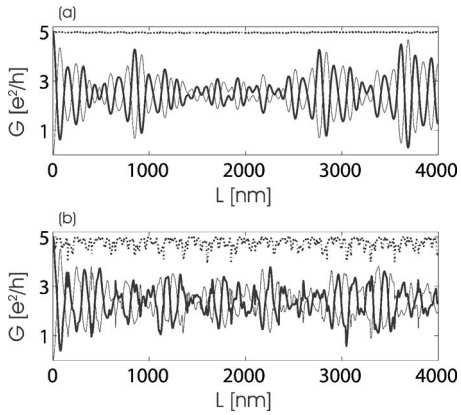


FIG. 7. Total conductance $G$ (dotted line), spin-up conductance $G^{\uparrow\uparrow}$ (thick solid line), and spin-down conductance $G^{\downarrow\uparrow}$ (thin solid line) as a function of the length $L$ of the SOI region with the width $w=100$ nm and the SOI strength $\alpha=33\times10^{-12}$ eV m: (a) the results for the Fermi energy at $E_F=28.5$ meV and (b) the results for the Fermi energy $E_F=32$ meV.

The above results clearly indicate that although the quantization characteristics of the total conductance show a weak dependence on the SOI strength, the behaviors of the two spin-dependent conductances and the spin polarization depend strongly on the SOI strength. It is this SOI dependence of the spin-polarized conductances that has been proposed to be employed in the realization of spin transistor devices. To give a more complete account for this SOI dependence, we show in Fig. 4 the calculated total conductance, $G$, and spin-dependent conductances, $G^{\uparrow\uparrow}$ and $G^{\downarrow\uparrow}$, as a function of the SOI strength $\alpha$ at two fixed Fermi energies. Figure 4(a) shows the results for $E_F=6.5$ meV. At this Fermi energy, the total conductance, $G$, stays at a quantization plateau [see the thin solid line in Fig. 4(a) and also Figs. 2 and 3]. However, the two spin-dependent conductances, $G^{\uparrow\uparrow}$ and $G^{\downarrow\uparrow}$, show rather regular oscillations. Thus a good modulation of the spin-dependent conductances can be achieved with a multimode quantum waveguide, as long as the total conductance can be tuned to stay at a conductance plateau. Figure 4(b) shows the results of the calculations for $E_F=7.9$ meV, at which the total conductance stays close to resonance dips. It can be seen that with increasing SOI strength $\alpha$, the two spin-dependent conductances, $G^{\uparrow\uparrow}$ and $G^{\downarrow\uparrow}$, still show rather regular oscillations, except at those $\alpha$ values where the total

conductance, $G$, shows sharp dips. Similar results are found for energies corresponding to five subbands open (see Fig. 5). These results have an important implication in terms of device technology: it is not absolutely required to have a single-mode conductor in order to realize a well-controlled spin transistor device.

Finally, we discuss the results of the calculations as a function of the SOI region length $L$, shown in Figs. 6 and 7. In these calculations, the SOI strength has been set to $\alpha = 33 \times 10^{-12}$ eV m, but the same Fermi energies as in Fig. 4, i.e., $E_F = 6.5$ and 7.9 meV, and in Fig. 5, i.e., $E_F = 28.5$ and 32 meV, have been assumed, respectively. It is clearly seen that at $E_F = 6.5$ meV [Fig. 6(a)], the total conductance stays at a plateau and only shows a weak dependence on the length $L$. It can also be seen from the figure that with increasing length $L$, the two spin-dependent conductances show regular oscillations. However, the amplitudes of the oscillations are strongly $L$-dependent and are approximately varied periodically as the SOI region length $L$ increases. This beating phenomenon of the spin-dependent conductances has already been reported in Ref. 5 and can be understood approximately as a result of the sum of the two individual transmissions through the first and second subbands, which oscillate with different frequencies. However, in strong contrast, the total conductance at $E_F = 7.9$ meV shows strong, irregular oscillations [Fig. 6(b)]. The same goes for the two spin-dependent conductances. These irregular fluctuations result again from strong intersubband coupling. At $E_F = 28.5$ meV, five subbands are open for conduction. The intersubband interaction is then expected to be strong and of a complicated nature. It is therefore not obvious that the above simple sum of contributions is valid. However, it is seen in Fig. 7(a) that some regular beating patterns as a function of length exist when the Fermi energy is on a conductance plateau. At $E_F = 32$ meV, an energy close to a high-index subband edge, these regular beating patterns are again destroyed [Fig. 7(b)], due to the strong intersubband coupling.

### B. Rashba superlattice

The study is now extended to the structure of a periodic array of $N$ units in the Q1D waveguide of width $w$ (see the inset of Fig. 8). Each unit consists of a region of length $L_1$ with finite SOI and a region of length $L_2$ with vanishing SOI. The period of the array structure is then $L_1 + L_2$. Such a structure has previously been studied using a transfer-matrix method.[5] However, the study was made under the assumption that only the two lowest subbands are involved in the transport and the calculations were performed in a truncated basis consisting of only two sublevels. Thus the contribution to the localized states in the superlattice region from the evanescent states and the effects of interaction with high-energy subbands are neglected. Here, to further demonstrate the power of our scattering-matrix formalism, we study the spin-dependent electron transport in regimes, where multiple subbands are open for conduction, with a basis set as large as necessary to obtain a desired convergence in the calculated quantities.

The total conductances, $G$, calculated for structures with $L_1 = L_2 = 100$ nm, $\alpha = 33 \times 10^{-12}$ eV m, $w = 100$ nm, and $N = 1$, 2, and 10 units are plotted in Fig. 8 as a function of the Fermi energy $E_F$. For one unit ($N = 1$), the conductance shows similar behavior as in Fig. 3(a) and is included for reference. With two units ($N = 2$), regions of suppressed conductance start to form on the conductance plateaus. For ten units ($N = 10$), these conductance suppression regions have developed into gaps, indicating the formation of minibands in the superlattice region. At each side of a conductance gap there are regular high-frequency oscillations. These oscillations appear as a result of electron transmission through the miniband states which have a discrete nature for the superlattice with a finite number of periods. Such features are generally expected for periodic structures (see, for example, Ref. 18).

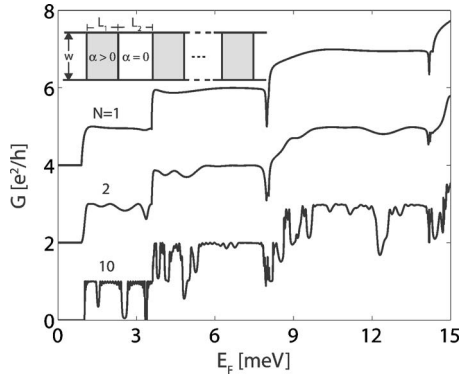


FIG. 8. Total conductance $G$ as a function of the Fermi energy $E_F$ for a Rashba superlattice with $\alpha = 33 \times 10^{-12}$ eV m, $L_1 = L_2 = 100$ nm, $w = 100$ nm, and $N = 1$, 2, and 10 units. The plots have been offset for clarity. The inset is a schematic illustration of the Rashba superlattice structure.

It is now interesting to ask whether the spin-dependent conductances show similar features as the total conductance of Fig. 8. In Fig. 9 we plot the individual spin conductances for the structures with $N = 2$, 3, 5, and 10 units. Here the plots for $N = 3$ and $N = 5$ units have been added to show the development. For the superlattice structure with two units, the spin-dependent conductances show rather simple behaviors except close to the subband edges [Fig. 9(a)]. For the superlattices with an increasing number of units, the spin-dependent conductances develop and show complex behaviors with regions of slow oscillations as well as regions of rapid oscillations [Figs. 9(b)–9(d)]. The slow oscillations occur at energies away from the onsets of subbands. However, the rapid oscillations are found at energies close to the onsets of subbands with the subband index $n \geqslant 2$. It is very interesting to note that these spin-dependent oscillations are not found in the total conductance (Fig. 8), indicating that a conduction peak for one spin orientation coincides with a conduction dip for the opposite spin orientation. Thus the rapid oscillations originate from strong spin scattering by localized states in the superlattice region. Since the rapid oscillations appear at energies close to an edge of a subband with subband index $n \geqslant 2$, the localized states contain significant contributions from high-index subbands in the SOI regions, in difference from the miniband states which are formed from a single subband (or, in other words, the subbands of the same index in the entire superlattice region). Thus these localized

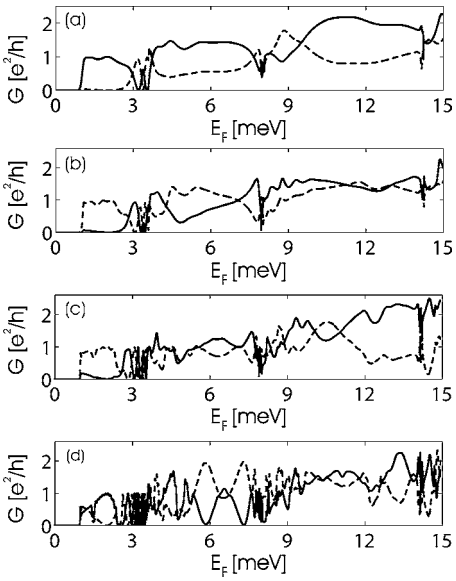


FIG. 9. Spin-up conductance $G^{\uparrow\uparrow}$ (solid line) and spin-down conductance $G^{\downarrow\uparrow}$ (dashed line) as a function of the Fermi energy for the Rashba superlattice structure with $\alpha=33\times10^{-12}$ eV m, $L_1=L_2=100$ nm, $w=100$ nm, and (a) $N=2$, (b) $N=3$, (c) $N=5$, and (d) $N=10$ units.

states need to be represented by including many high-energy subbands in the calculations, and a two-subband model may fail to produce the rapid oscillations in the spin-dependent conductances. In Fig. 10 we plot the spin polarization corresponding to Fig. 9. Here the fast oscillations are again seen in the energy regions where the spin-dependent conductances show rapid oscillations. The oscillations in the spin polarization close to the second subband edge are especially clear. Here, for every unit added, more oscillation peaks in the spin polarization are found.

## IV. CONCLUSIONS

We have presented a formulation of the scattering matrix method for spin-dependent electron transport in a quantum waveguide. In the formulation, only the Rashba SOI has been taken into account. However, the incorporation of the Dresselhaus SOI and an applied magnetic field in the formulation is straightforward. The transfer matrices needed in the implementation of the scattering-matrix method has been derived. In particular, we have represented all the required Hamiltonian matrices in terms of the transverse spatial eigenstates and the spin eigenstates of the leads. Thus the method has great flexibility and can easily be applied to systems with complex geometrical structure, potential distribution, SOI strength profile, etc. Also, the method is numerically stable and can be employed to treat spin-dependent multisubband scattering processes accurately. As applications, the method has been implemented in the studies of spin-dependent electron transport in Q1D conductors, with a region of the Rashba SOI and with a region containing a Rashba superlattice, made from a semiconductor heterostructure. The total conductance, spin-dependent conductances, and spin polarization of the device system have been calculated for electrons injected in a pure spin-polarized, say spin-up, state from a lead into the SOI region.

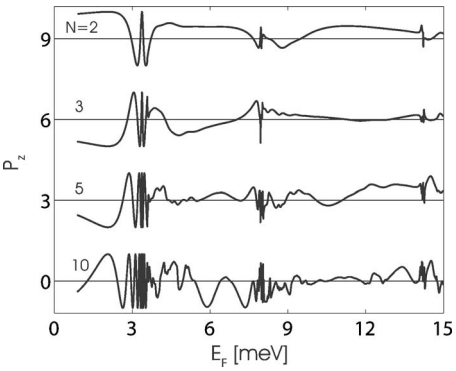


FIG. 10. Spin polarization $P_z$ as a function of the Fermi energy $E_F$ for the Rashba superlattice structure in Fig. 9. The plots, with the zero polarization indicated by a horizontal line in each plot, have been offset for clarity.

For the Q1D conductor with a single region of the Rashba SOI, the calculations show that at weak SOI strengths, the main effect of the SOI is to entangle the spin-up and spin-down states of an electron and to rotate the electron spin as the electron goes through the SOI region. As a result, the spin polarization for a given structure is roughly Fermi-energy independent and the subband coupling has a negligible effect on the spin polarization. At strong SOI strengths, the spin-dependent conductance as well as spin polarization show strong Fermi-energy dependences. It is shown that the influence of SOI-induced subband coupling on the spin-dependent transport is particularly strong at Fermi energies close to the onsets of subbands (with the subband index $n \geqslant 2$). However, at a Fermi energy, where the total conductance is at a conductance plateau, the spin-dependent conductances still show rather regular oscillations with increasing SOI strength $\alpha$ or SOI region length $L$. Our results indicate that to achieve a well-controlled spin transistor device, it may not be absolutely required that the SOI-incorporated waveguide conductor be operated in the single-mode conduction regime.

For the Q1D conductor modulated by a periodic array of strong Rashba SOI regions, the total conductance shows the standard superlattice behavior. However, the spin-dependent conductances and the spin polarization show complex behavior with regions of slow oscillations and regions of rapid oscillations. As in the Q1D conductor with a single SOI region, the slow oscillations are found in the energy regions where the total conductance is at a plateau. The rapid oscillations appear at energies close to the onsets of subbands with the subband index $n \geqslant 2$. These oscillations originate from strong spin scattering by localized states in the SOI-modulated superlattice region, which, in difference from the miniband states formed within a single subband, contain significant contributions from high-energy subbands. Because of the complex nature of the spin-dependent conductances, a Rashba SOI-modulated superlattice may hardly be used as a well-controlled spin-modulating device, although it could be used for standard superlattice applications.

**ACKNOWLEDGMENTS**

The authors thank Dr. Feng Zhai for stimulating discussions. This work, which was performed in the Nanometer Structure Consortium at Lund University, was supported by the Swedish Research Council (VR) and by the Swedish Foundation for Strategic Research (SSF).

*Electronic address: lebo.zhang@ftf.lth.se
†Electronic address: patrik.brusheim@ftf.lth.se
‡Corresponding author. Electronic address: hongqi.xu@ftf.lth.se

[1] S. A. Wolf, D. D. Awschalom, R. A. Buhrman, J. M. Daughton, S. von Molnr, M. L. Roukes, A. Y. Chtchelkanova, and D. M. Treger, Science **294**, 1488 (2001).
[2] Jun Wang, H. B. Sun, and D. Y. Xing, Phys. Rev. B **69**, 085304 (2004).
[3] F. Mireles and G. Kirczenow, Phys. Rev. B **64**, 024426 (2001).
[4] X. F. Wang and P. Vasilopoulos, Phys. Rev. B **68**, 035305 (2003).
[5] X. F. Wang, Phys. Rev. B **69**, 035302 (2004).
[6] G. Feve, W. D. Oliver, M. Aranzana, and Y. Yamamoto, Phys. Rev. B **66**, 155328 (2002).
[7] M. Cahay and S. Bandyopadhyay, Phys. Rev. B **69**, 045303 (2004).
[8] M. W. Wu, J. Zhou, and W. Shi, Appl. Phys. Lett. **85**, 1012 (2004).
[9] E. G. Mishchenko and B. I. Halperin, Phys. Rev. B **68**, 045317 (2003).
[10] R. M. Potok, J. A. Folk, C. M. Marcus, and V. Umansky, Phys. Rev. Lett. **89**, 266602 (2002).
[11] J. C. Egues, G. Burkard, and D. Loss, Appl. Phys. Lett. **82**, 2658 (2003).
[12] S. K. Upadhyay, R. N. Louie, and R. A. Buhrman, Appl. Phys. Lett. **74**, 3881 (1999).
[13] S. Datta and B. Das, Appl. Phys. Lett. **56**, 665 (1990).
[14] U. Zülicke and C. Schroll, Phys. Rev. Lett. **88**, 029701 (2002).
[15] T. Matsuyama, C.-M. Hu, D. Grundler, G. Meier, and U. Merkt, Phys. Rev. B **65**, 155322 (2002).
[16] H. Tamura and T. Ando, Phys. Rev. B **44**, 1792 (1991).
[17] H. Xu, Phys. Rev. B **52**, 5803 (1995).
[18] H. Xu, Phys. Rev. B **50**, 8469 (1994).
[19] David Yuk Kei Ko and J. C. Inkson, Phys. Rev. B **38**, 9945 (1988).
[20] H. Xu and W. Sheng, Phys. Rev. B **57**, 11903 (1998); Superlattices Microstruct. **25**, 79 (1999).
[21] I. A. Shelykh and N. G. Galkin, Phys. Rev. B **70**, 205328 (2004).
[22] D. Csontos and H. Q. Xu, Appl. Phys. Lett. **77**, 2364 (2000).